HHS Public Access

Author manuscript

Neuroimage. Author manuscript; available in PMC 2022 November 01.

Published in final edited form as:

Neuroimage. 2022 November 01; 261: 119499. doi:10.1016/j.neuroimage.2022.119499.

Representational coding of overt and covert orienting of visuospatial attention in the frontoparietal network

Tingting Wu[a], **Melissa-Ann Mackie**[b], **Chao Chen**[c], **Jin Fan**[a,*]

[a]Department of Psychology, Queens College, City University of New York, Queens, NY 11367, United States

[b]Department of Psychiatry and Behavioral Sciences, Northwestern University Feinberg School of Medicine, Chicago, IL 60611, United States

[c]Departments of Biomedical Informatics, Stony Brook University, Stony Brook, NY 11794, United States

Abstract

Orienting of visuospatial attention refers to reallocation of attentional focus from one target or location to another and can occur either with (overt) or without (covert) eye movement. Although it has been demonstrated that both types of orienting commonly involve frontal and parietal brain regions as the frontoparietal network (FPN), the underlying representational coding of these two types of orienting remains unclear. In this functional magnetic resonance imaging study, participants performed a task that elicited overt and covert orienting to endogenously or exogenously cued targets with eye-tracking to monitor eye movement. Although the FPN was commonly activated for both overt and covert orienting, multivariate patterns of the activation of voxels in the FPN accurately predicted whether eye movements were involved or not during orienting. These overt- and covert-preferred voxels were topologically distributed as distinct and interlaced clusters in a millimeter scale. Inclusion of the two types of clusters predicted orienting type more accurately than one type of clusters alone. These findings suggest that overt and covert orienting are represented by interdependent functional clusters of neuronal populations in regions of the FPN, which might reflect a generalizable principle in the nervous system for functional organization of closely associated processes.

Keywords

Orienting of attention; Overt; Covert; Frontoparietal network

*Corresponding author at: Department of Psychology, Queens College, The City University of New York, 65-30 Kissena Blvd., Queens, NY 11367 United States, jin.fan@qc.cuny.edu (J. Fan).

Author Contributions

J.F. and M.M. designed the experiments and were involved in fMRI data collection; T.W. and M.M. analyzed the data; C.C. contributed to the characterization of the topologic map. All authors discussed the results and contributed to the writing of the report.

Declaration of Competing Interest

The authors declare no competing financial interests.

Supplementary materials

Supplementary material associated with this article can be found, in the online version, at doi: 10.1016/j.neuroimage.2022.119499.

1. Introduction

Allocation of attention toward a source of external sensory it is known as the orienting function of attention (Posner, 1980, 2016; Wright and Ward, 2008) and can be executed with or without saccadic eye movements, called overt and covert orienting, respectively (Posner, 1980, 2016). Clarifying the degree of the relationship between eye movement and covert orienting is critical to understand the origin and nature of attention. The logical possibilities of relationship between them are on a continuum with complete dependence and complete independence as the two extremes (Posner, 1980). Complete dependence asserts that eye movement (here we use the term overt orienting inter-changeably with attention guided eye movement) and covert orienting are inextricable processes supported by the same underlying mechanisms (Posner, 1989). For example, the premotor theory of attention proposed that orienting of attention arises from saccade preparation (Rizzolatti et al., 1987; Rizzolatti et al., 1994). In contrast, complete independence posits that eye movements and covert orienting are orthogonal processes supported by different anatomical substrates (Ponser, 1980).

Anatomical overlap found in neuroimaging studies provided some support for the dependence between overt and covert orienting. It has been demonstrated that both overt and covert orienting of attention are reliably associated with increased brain activation in a large-scale frontoparietal network (FPN) (Beauchamp et al., 2001; Corbetta, 1998; Corbetta et al., 1998; De Haan et al., 2008; Fairhall et al., 2009; Gitelman et al., 2002; Grosbras et al., 2005; Nobre et al., 2000; Nobre et al., 1997), which is comprised of frontal regions around the intersection of the middle frontal gyrus with the precentral gyrus (named frontal eye fields, FEFs) and parietal regions near and along intraparietal sulcus (IPS). This network is also named the “dorsal attention network” or “dorsal FPN” in literature related to dorsal and ventral pathways of attention (i.e., Ptak et al., 2017; Shulman et al., 2010; Szczepanski et al., 2013), while the ventral network is comprised of anterior insular cortex and anterior cingulate cortex. Here the term FPN is utilized as in the literature of overt and covert orienting. The FPN has been considered as a “source” of orienting in the brain that executes attentional control by sending bias signals to modulate activity in visual areas and guiding the generation of oculomotor actions (Corbetta et al., 1998; Moore et al., 2003; Petersen and Posner, 2012; Posner and Petersen, 1990). However, single cell recording in monkeys provided compelling evidence at the neuronal level that separate populations of neurons within the FEF (Awh et al., 2006; Bruce and Goldberg, 1985; Bruce et al., 1985; Cohen et al., 2009; Sato and Schall, 2003; Schall, 1991) (e.g., visual and movement neurons) drive attentional location selection and gaze control (Schall, 2004; Thompson et al., 2005). This dissociation provided support for the independence between overt and covert orienting.

In contrast to the two extreme models of complete dependence and complete independence between overt and covert orienting, a more moderate model of an interdependent relationship has been proposed with resources or computations shared at certain but not all stages by overt and covert orienting (Belopolsky and Theeuwes, 2012; Casteau and Smith, 2019; Corbetta et al., 1998; Hunt and Kingstone, 2003; Jonikaitis and Moore, 2019; Posner, 1980). It has been argued that this relationship is supported by a large-scale functional segregation of the FPN, with the IPS more involved in orienting and the FEF

more involved in t eye movement, or supported by a partial segregation as different subdivisions within regions of the FPN (e.g., distinct “overt” and “covert” areas within the FEF and IPS) (Corbetta, 1998; Posner, 1980). In contrast, single cell recording studies revealed a continuum of visual-movement functions among neurons within the FEF (Moore et al., 2012), suggesting that there might be an fine-scale interdependent representational coding by populations of neurons with different preferences for overt and covert orienting within the regions of the FPN. The neural mechanism, i.e., whether large-scale functional segregation or fine-scale representational coding underlies this interdependent relationship, however, remains elusive.

Methodological data-analytic techniques for functional magnetic resonance imaging (fMRI) data provide advanced tools for the decoding of the representation of different cognitive processes in functionally overlapping regions of the brain. Compared to the conventional univariate analysis with general linear modeling (GLM) typically used to identify and localize brain regions involved in a certain process, multivariate pattern analysis (MVPA) has a specific advantage in decoding multidimensional representation as patterns of activation in voxels or regions associated with different processes in a commonly involved region or network (Davis et al., 2014; Haxby, 2012; Peelen and Downing, 2007; Peelen et al., 2006). Although the millimeter-level spatial resolution of the voxels in fMRI is much lower than the below-millimeter columnar level neural population, patterns of voxel-wise activation in a brain area decoded by MVPA can reflect the underlying columnar level organization of representational codes for a specific cognitive process (Boynton, 2005; Haynes and Rees, 2005; Kamitani and Tong, 2005; Misaki et al., 2013). Therefore, the representation ecoding of overt and covert orienting in the FPN can be examined using MV-PAu. Enhancement of spatial resolution of fMRI data acquisition would facilitate the detection of the fine-scale pattern of neural representation (Gardumi et al., 2016; Mandelkow et al., 2017; Swisher et al., 2010).

In this study, we designed a cue-target attention task to manipulate visuospatial overt and covert orienting by instructing participants either to move their eyes or maintain central fixation following a location cue. In addition, to examine generalizability of the decoding of overt and covert orienting, we also manipulated the cue type: voluntary “endogenous” cueing that follows a goal-oriented decision to attend to a specific location versus reflexive “exogenous” cueing in which attention is captured via a salient cue (Müller and Rabbitt, 1989; Posner, 1980, 2016; Posner et al., 1985). Brain activation associated with the task manipulation was measured using accelerated multiband fMRI, together with simultaneous eye-tracking to monitor participants’ eye movement. A GLM was conducted first to test the involvement of the FPN in overt and covert orienting. MVPA was then performed to test whether the overt versus covert orienting could be decoded by voxel-wise patterns of activation within the FPN in a trial-by-trial manner, and to estimate the patterns (i.e., the representation) of voxels with different preferences to overt and covert orienting. To further characterize the topological organization of the representation in space, we decomposed the pattern into overt- and covert-preferred clusters of voxels by using Morse theory and its discrete version (Delgado-Friedrichs et al., 2015; Forman, 2002; Milnor, 1963) and then quantified the interleaving pattern of the two types of clusters using spatial statistics (Diggle et al., 1976; Gómez-Rubio, 2016; Loosmore and Ford, 2006).

The existence of interdependent representational coding of overt and covert orienting in the FPN would be supported by the findings that (1) the FPN was commonly activated in both overt and covert orienting to demonstrate the shared resources for these two types of orienting; (2) the pattern of voxel-wise activation in the FPN could be decomposed into overt- and covert-preferred voxels, and (3) a successful classification of overt and covert orienting could be achieved by overt- and covert-preferred voxels solely, and would be significantly improved when combining the two types of voxels, to demonstrate the distinct and interactive representation within the FPN. The organization of this representation (i.e., large-scale functional segregation or fine-scale representational coding) could be further examined by quantifying the topological distribution of overt- and covert-preferred clusters of voxels.

2. Method

2.1. Participants

Twenty-four adult participants completed the experiment. Data from two participants were excluded due to technical issue in eye-tracking data collection, two more participants were excluded due to excessive head motion, and three participants were excluded for excessive drowsiness in the scanner impacting either the ability to collect eye tracking data or their behavioral performance. The final sample size was $n = 17$ (9 females and 8 males), each with no history of neurological or psychiatric disorder and a full-scale intelligence quotient (FSIQ) above 80. Power analysis conducted using G*Power 3.1 (Faul et al., 2009) (RRID : SCR_013726, http://www.gpower.hhu.de/) demonstrated that the final sample had sufficient power to detect the core effects of interest (see Supplementary Results for details). The Institutional Review Board of the City University of New York and Icahn School of Medicine at Mount Sinai (ISMMS) approved the protocol and written informed consent was obtained from each participant.

2.2. The design of the overt and covert orienting task

The overt and covert orienting task (Fig. 1) was designed to investigate overt and covert orienting of attention in response to cues that induce both endogenous and exogenous orienting. A fixation set, comprised by eight possible cue/target locations presented as circles (each with diameter of 3.9°) arranged around a fixation cross (diameter of 1.9°) with the visual angle as 10° from the center of each circle to the fixation cross, was presented all through each run. This task was comprised of a 2 (Orienting: overt, covert) × 2 (Cueing: endogenous, exogenous) factorial design, with four corresponding trial types (i.e., overt-endogenous, overt-exogenous, covert-endogenous, covert-exogenous). The task consisted of four runs of trials and each run consisted of 16 blocks with 8 trials in each block. Only one trial type was presented in each block, indicated by the color of fixation cross: at the beginning of each block, the fixation cross either changed to green to indicate the participant to move eyes towards the cued-location after the cue and quickly return to central fixation after making a response in each trial (overt block), or changed to red to indicate to the participant to maintain central fixation during the entire block (covert block). The fixation cross remained colored throughout the entire block. These blocks were presented in a random order, and blocks in each run were separated by 15-s fixation periods.

Each run began with a 15-s fixation period and ended with a 30-s fixation period. The entire task was comprised of a total of 512 trials, and the task lasted approximately 50 minutes.

Each trial within a block began with a variable fixation period of 0 to 1000 ms. Then one of the circles was cued either by an arrow (with the length as 2.9°) superimposed on the fixation cross location pointing to the circle (endogenous cue), or by a change in luminance at the location circle (exogenous cue). The cued location was randomized within each block, and the cue period lasted 200 ms. After a 600-ms cue-to-target interval, a target arrow appeared within the cued circle and was presented for 200 ms, followed by another variable fixation period of 2000 to 3000 ms. Each trial lasted 4000 ms. The length of the target arrow was identical to the diameter of the circle. Participants were required to respond to the direction of the target arrow by pressing a button (the left index finger for a left response, and the right index finger for a right response). The response window was 1700 ms starting at the target onset.

2.3. Eye-tracking data acquisition

Eye movements during the task were recorded using a ViewPoint Eyetracker (2010, Arrington Research, Scottsdale, AZ) with video capture goggle system at a 60-Hz sampling rate. The position of the eye camera was adjusted to obtain an image of the eye in which the pupil was in the center of eye camera window when the participant was looking straight ahead, and the corners of the eye were at the horizontal edges of the camera window. The spatial resolution of the recording window was 1600 × 1200. Sixteen-point calibration was completed until an accurate calibration was obtained for each participant. Pupil location was achieved at a luminance threshold of 0.25 and a scan density setting of 7. Pupil segmentation method was set as “ellipse”. Data was online smoothed as simple moving average with 4 smoothing points.

2.4. fMRI data acquisition

All MRI scans were acquired on a 3T Siemens Magnetom Skyra scanner with a 16 phase-array channel head coil at ISMMS. All image volumes were acquired along the axial plane parallel to the anterior commissure-posterior commissure (AC-PC). Four runs of T2*-weighted image volumes were acquired with a multiband accelerated echo-planar imaging (EPI) sequence with the following parameters: 72 axial slices 2.3 mm thick, repetition time (TR) = 1200 ms, echo time (TE) = 31.4 ms, multiband acceleration factor = 6, flip angle = 60°, field of view (FOV) = 224 mm, echo spacing = 0.65 ms, matrix size = 98 × 98, voxel size = 2.3 × 2.3 × 2.3 mm. A single-band image (SBRef image) was acquired at the beginning of each run, and then two dummy volumes were acquired to allow for equilibration of T1 saturation effects, followed by 665 volumes. After the EPI scans, two field maps were acquired using a double-echo gradient echo sequence, with the following parameters: 72 axial slices 2.3 mm thick, TR = 731 ms, echo spacing = 0.65 ms, flip angle = 50°, FOV = 224 mm, matrix size = 90 × 90, voxel size = 2.5 × 2.5 × 2.3 mm. A field-map as opposite phase encoded EPI was acquired as the difference in distortion between two acquisitions with opposite phase encoding directions with TE = 4.92 ms. A high-resolution T1-weighted anatomical image volume of the whole brain was acquired with a magnetization-prepared rapid gradient-echo (MPRAGE) sequence with the following

parameters: 176 axial slices 0.9 mm thick, TR = 2200 ms, TE = 2.5 ms, flip angle = 8°, FOV = 240 mm, matrix size = 256 × 256, voxel size = 0.9 × 0.9 × 0.9 mm.

2.5. Procedure

Participants were screened for eligibility in an initial session, in which a 3-subtest WAIS-IV short form (Vocabulary, Symbol Search, and Figure Weights) (Wechsler, 2008), Edinburgh Handedness Inventory (Oldfield, 1971), and Structured Clinical Interview for DSM-IV (SCID-IV) (Spitzer et al., 1994) were administered. They also completed a screening form assessing the presence of metal in the body as well as personal and family medical and psychiatric history. Participants who passed the screening then returned for the scan session on another day. Each participant was informed about the task instructions, and was then trained on the task in an MRI simulator, in which they completed two runs of trials. This was immediately followed by the scan session. The task was compiled and run on a PC using E-Prime software (Psychology Software Tools, Pittsburgh, PA). Stimuli were presented on a liquid crystal monitor mounted at the back of the scanner bore (refresh rate: 60 Hz; screen resolution: 1024 × 768). Participants viewed the screen through a head-coil mounted mirror. The view distance was 238 cm. MRI compatible lenses were provided to participants who required vision correction. Participants' responses were collected using a fiber optic button system with two button response gloves (BrainLogic, Psychology Software Tools) placed under their left and right hands.

2.6. Eye-tracking data analysis

Eye-tracking data were analyzed with the GazeAlyze toolbox (Berger et al., 2012) for off-line preprocessing. The period from the cue onset to 1000 ms after the target offset in each trial was segmented, with the period between the cue onset and the target onset as the window of interest, and the 1000 ms post-target periods as the reference for the drifting correction. Blink detection and smoothing were conducted with default parameters. The coordinates of the gaze position in each trial were generated after these preprocessing steps.

Artifact detection was conducted using an in-house Matlab script. Slow drifting within each run was corrected using a moving window approach, in which the mean coordinates across 32 trials before and after each trial were subtracted from the coordinates of gaze position in that trial. The area of interest of the covert condition was defined as a circle with the diameter as 1/4 of the length of the recording window, and the area of interest of the overt condition was defined as the area outside the areas of interest of covert. Trials with the gaze position located outside the areas of interest of the corresponding condition were identified as outliers. For each task condition, the coordinates of gaze position in trials with the cue and target appearing at each of the eight circles were calculated separately. Trials with the coordinates outside 3 standard deviation (SD) of each target location in each task condition were also identified as eye-tracking outliers. All trials identified as outliers were removed from all of the following analyses. There were 80.0 ± 16.1% (mean ± SD) trials remaining after the artifact detection and outlier exclusion. The exclusion rate did not significantly differ between the overt (18.9 ± 15.6%) and covert (19.9 ± 20.1%) conditions, $t(16) = 0.092$, $p = .928$. The mean and SD of the coordinates in the remaining trials were calculated for each target location in each task condition. The eye-movement distance (in visual angle)

from the gaze position to the center of the window was then calculated. A 2 (Orienting: overt, covert) × 2 (Cueing: endogenous, exogenous) analysis of variance (ANOVA) was conducted on the eye-movement distance.

2.7. Behavioral analysis

The response accuracy was calculated for trials with valid eye-movements, as the percentage of trials with correct responses out of the total number of trials in each condition. RT in each trial was measured as the interval between the target onset and the subsequent button press made within the 1700-ms response window. Mean and SD of RTs in each condition were calculated for each participant. Trials with no response or incorrect responses and trials identified as eye-tracking outliers were excluded from the RT analyses. Trials with RT exceeding 3 SD of the mean RT across the remaining trials in each condition were considered as RT-outliers and were also excluded from the RT analyses. There were 98.2 ± 0.01% trials remained after this RT trimming. A 2 (Orienting: overt, covert) × 2 (Cueing: endogenous, exogenous) ANOVA was conducted on the RT.

2.8. Image preprocessing

Functional MRI preprocessing and statistical modeling were conducted using the statistical parametric mapping package (SPM12, Well-come Trust Centre for Neuroimaging, London, UK), following the Human Connectome Project (HCP) minimal preprocessing pipeline (Glasser et al., 2013). Fieldmap correction was first conducted for all EPI images. EPI images in each run were realigned to the SBRef images and all SBRef images were realigned to the SBRef image in the first run. The mean SBRef image across all runs was then co-registered to the T1 image, spatially normalized to the Montreal Neurological Institute (MNI) ICBM 152 space based on normalization parameters of the T1 image, and resampled to a voxel size of 2 × 2 × 2 mm. To examine the experimental effect on brainstem regions (such as superior colliculus) and cerebellum, the normalized EPI images were further co-registered to both MNI ICBM 152 EPI template and the EPI template weighted by the brainstem mask (Xuan et al., 2016). All normalized EPI images were also spatially smoothed with an 8 × 8 × 8 mm full-width-at-half-maximum (FWHM) Gaussian kernel for the GLM. Normalized but unsmoothed data was used in the MVPA.

2.9. Localization of brain regions involved in overt and covert orienting

We applied a single-trial analysis protocol (Choi et al., 2012; Kinnison et al., 2012; Rissman et al., 2004; Wu et al., 2018) to identify brain regions involved in overt and covert orienting as the regions showing significant activation increase in each trial and in the overt and covert conditions. Conjunction analysis was then conducted to identify regions commonly involved in both conditions, and disjunction analysis was conducted to identify regions specifically involved in each condition. We also compared the results of single-trial analysis to the conventional GLM to validate the single-trial analysis. These analyses were conducted in a whole-brain voxel-wise manner, and the following analyses focused on the frontal and parietal clusters of the FPN (including the FEF and the IPS) identified in the conjunction analysis. The single-trial signal extraction enabled us to test the classification power of the activation of the voxels in the regions of the FPN in a trial-by-trial manner in the MVPA. This protocol, rather than the block-wised analysis, was applied because only trials with

gaze located on the target circle and with correct response were included in the MVPA analyses.

2.9.1. Conventional general linear modeling—First-level (subject-level) GLM was conducted for the EPI images by regressing the observed event-related blood oxygenation level-dependent (BOLD) signals on task-related regressors to identify the brain regions which showed the hemodynamic response as a function of task events for each participant (Friston et al., 1994). For each run, onsets of cues in each task condition were modeled as a train of delta functions, and then these onset vectors were convolved by a SPM basis function of hemodynamic response (HRF) (Friston et al., 1998) to create four regressors of interest. Only trials with correct responses and not identified as eye-tracking outliers were included. In addition, onset vectors for cues in trials with incorrect responses or identified as eye-tracking outliers were also constructed for each condition, if any, and then convolved with the HRF to create nuisance regressors, resulting in a range of 0 to 8 nuisance regressors in each run. The six motion parameters generated during realignment and one regressor to indicate runs were entered as nuisance covariates for each run. Low-frequency drifts in signal were removed using a high-pass filter of 256 s. Serial correlation was estimated using an autoregressive AR(1) model. The GLM was estimated and the images of parameter estimates (beta images) were obtained. This model did not separate the activation associated with the processing of cue and target because the cue-to-target interval was fixed in the task. The estimated parameters represent the overall activation change during the entire process of attention orienting, including both cue- and target-related activation.

Orthogonal polynomial contrasts across beta images of the four regressors of interest (i.e., overt-endogenous, overt-exogenous, covert-endogenous, covert-exogenous) were applied to identify brain regions that: 1) showed significant increase in activation in overt conditions versus fixation baseline (contrast vector: [0.5, 0.5, 0, 0]) and covert conditions versus fixation baseline (contrast vector: [0, 0, 0.5, 0.5]), and 2) showed significant different between overt and covert conditions (overt > covert: [0.5, 0.5, −0.5, −0.5], covert > overt: [−0.5, −0.5, 0.5, 0.5]). It is worth noting that although the estimated BOLD signal included activation associated with both cue- and target-related process, the location of the target was counterbalanced between the overt and covert conditions and the cue was 100% valid, therefore the second contrast should not be affected by the difference in target-related process. The contrast vectors were normalized across all runs. The contrast images from all participants were then entered into a second-level group analysis for each effect, with random-effects statistical model in which the cue effect was the fixed effect and participants was the random effect. The conjunction between the effects of overt-minus-fixation-baseline and covert-minus-fixation-baseline was examined to identify common regions of activation in the overt and covert conditions. The threshold of significance for each test was set as an uncorrected voxel-wise level $p < 0.001$ for the height with a contiguous voxel extent threshold (k) that was estimated by random field theory to correct for multiple voxel comparisons at a cluster-wise level of $p < 0.05$. Disjunction analysis was conducted to identify regions with an increase in activation specifically in the overt or the covert condition by masking out activation in one condition (e.g., covert) when testing for activation in the

other condition (e.g., overt), with the threshold of the exclusive mask as uncorrected $p < 0.05$.

2.9.2. Single-trial analysis—Single-trial extraction was conducted using a "extract-one-trial-out" approach (Choi et al., 2012; Kinnison et al., 2012; Padmala and Pessoa, 2011; Rissman et al., 2004), with its detection and estimation power demonstrated in our previous study (Wu et al., 2018). Specifically, a first-level GLM was constructed and estimated for each individual trial of interest. The regressors in this GLM were identical to the first-level GLM described above, except that the regressor of the condition containing the trial of interest was split into two regressors: 1) the regressor as the convolution of the HRF and the onset of cue in the trial of interest; and 2) the regressor as the convolution of the HRF and the onsets of cue in the rest of trials in this condition except for the trial of interest. The estimated beta image for the trial of interest was considered as the brain responses associated with the condition of the trial of interest. This routine was looped for trials with correct responses and not identified as eye-tracking outliers. Trials with a global mean beta value across all voxels that was above or below 3 SD of the mean across all remaining trials were defined as outliers and removed from the following analyses. Brain activation associated with overt and covert orienting were estimated as the averaged beta images across all trials in the corresponding condition.

First-level statistical analysis was conducted as an independent sample t-test of the overt versus covert comparison for beta values in each voxel in the FPN. The generated subject-level averaged beta images of overt and covert conditions were then entered into a second-level group analysis as a paired t-test. The effects of overt-minus-fixation-baseline, covert-minus-fixation-baseline, the conjunction and disjunction analyses of these two effects, and the comparison of overt versus covert were examined based on this second-level GLM. The significant threshold of each test was FWE corrected voxel-wise level $p < 0.05$ for the height with a contiguous voxel extent threshold (k) that was estimated by random field theory to correct for multiple voxel comparisons at a cluster-wise level of $p < 0.05$.

2.10. Classification of overt versus covert orienting based on activation in the regions of the FPN

We employed MVPA (Haxby et al., 2001; Haynes and Rees, 2005; Norman et al., 2006) to test whether overt and covert orienting of attention can be predicted based on activation of voxels in the regions of the FPN. The support vector machine (SVM) (Cortes and Vapnik, 1995), which is one of the most popular supervised machine learning methods, was used as the classifier. The linear SVM in this study modeled the relationship between the orienting type in each trial (target variable) as a weighted sum across the activation across voxels in an ROI of the FPN (input features). The linear model was adopted to reduce the risk of over-fitting caused by the much larger number of feature dimensions (e.g., the number of voxels) compared to the sample size (i.e., the number of trials) (Misaki et al., 2010). The linear SVM was implement using the "fitsvm" function in the Statistics and Machine Learning Toolbox of MATLAB. The frontal ROI (named as FEF) and the parietal ROI (named as IPS) were defined as the corresponding clusters that showed significant activation in the conjunction analysis, and the ROI of FPN was defined as the combination of these

two ROIs. Voxel-wise activation for each ROI was extracted from the single-trial beta maps estimated based on normalized but unsmoothed EPI images.

The input feature of the SVM was a $m \times n$ array, with each row as the vectorized activation of voxels in an ROI in each trial (m: number of trials, ranged from 195 to 485), and each column as the beta values of voxels in the ROI (n: number of voxels, 7423 for the FEF, 8953 for the IPS, and 16376 for the FPN). The values of each input feature were normalized across all trials (mean as 0 and SD as 1). The overt condition was coded as the negative class and covert condition was coded as the positive class. Here the number of trials in the overt and covert conditions were relatively balanced for all participants, with the ratio of covert conditions ranging from 49.1% to 53.8%, and therefore not expected to significantly bias the classifications. Classification decisions in linear SVM were computed through a linear combination of weights and input data: $\hat{y} = w^T x + b$, with x as the features, $\hat{y}$ as the expectation of the target variable, and w as the weight vector across features. The weight vector was estimated when searching the hyperplane with the largest margin between the two classes, as the best one that separates all data points of one class from the other class (Cortes and Vapnik, 1995). The trials were split into two independent sets: the training set and the testing set. The weight vector learned based on the training set was applied to the testing set to predict the class of each trial, in which a trial with $\hat{y}<0$ predicted as an overt trial and a trial with $\hat{y}>0$ predicted as a covert trial. The sign of the weight of each feature represents the response bias of that voxel, with a negative weight representing an overt preference and a positive weight representing a covert preference. The absolute value reflects the importance of this feature in the classification, with a bigger absolute value indicating a higher importance.

Ten-fold cross validation was employed to evaluate the performance of this binary classification, in which all trials were randomly divided into 10 folds, with 9 of them as the training set and the rest one as the testing set. The classifier trained based on the training set was then applied to predict the class of each trial in the testing set. There were four possible outcomes of the prediction: true positive (TP), true negative (TN), false positive (FP), and false negative (FN). The focal measure of the classification performance was the accuracy, i.e., (TP + TN) / (TP + FP + FN + TN). Other measures of the classification performance were also computed for each class, including precision = TP / (TP + FP), recall (sensitivity) = TP / (TP + FN), and F1 score = 2 × (recall × precision) / (recall + precision). These measures could reflect whether the classification was biased: an unbiased classification will reveal similar estimates between the two target classes for each measure. A total of 1000 permutations of 10-fold cross validation were performed for each participant. The average of each of the measures of outcomes was computed.

The null distributions of performance and weights were estimated by randomly shuffling the target classes in another 1000 permutations of 10-fold cross validation. For the measures of performance, the average of each measure was computed as the estimated chance level performance and then compared to the empirical measures across participants using paired t-tests. For the subject-level analysis of the weight, the distribution of the empirical weight values was compared to the null distribution for each feature as a two-sample t-test. Bonferroni correction was applied to correct for multiple comparison, resulting in a

corrected significant level of $p < .05$. The thresholded weight vector was mapped back to 3D MNI space based on the corresponding coordinates of each voxel to generate a thresholded weight map for each participant.

We did not apply similar analyses to examine the exogenous and endogenous differences because it is not the focus of this study. The main hypothesis of this study focuses on the encoding mechanisms of overt and covert orienting of attention, whereas there was no similar hypothesis for exogenous and endogenous attention. Additionally, exogeneous and endogenous attention are highly related to cueing and due to the fixed cue-target interval in this experiment, the cue- and target-related BOLD responses could not be separated.

To examine the impact of spatial smoothing on the classification performance, MVPA was also performed on voxel-wise activation extracted from the single-trial beta maps estimated based on spatially smoothed EPI images (FWHM = 8 × 8 × 8 mm). The classification performance of MVPA based on unsmoothed and smoothed EPI were compared as paired t-tests. To examine the potential impact of block structure on the classification performance, i.e., whether the temporal proximity between events contributed to the classification, a control analysis was performed for each ROI. In this analysis, all trials in 1 out of 10 blocks, rather than 1 out of 10 trials, were assigned as the testing set, while the rest of trials were assigned as the training set. In the corresponding permutation analysis for the baseline performance, trial labels were shuffled at block level, rather than trial level, to match the temporal adjacency of trials within blocks.

We also conducted a group-level analysis for the weight maps, in which empirical weight maps (unthresholded) were also compared to the chance level weight maps as a paired t-test (two-tailed) for each voxel within the ROI. Bonferroni correction was applied to correct for multiple comparisons, resulting in a corrected significance level of $p < .05$. To examine the similarity between the weight map and univariate activation map generated in the GLM, we transformed each map into a 1-d array and then computed the Pearson correlation coefficient between them. Here univariate activation maps estimated based on the unsmoothed single-trial images were used to make them comparable to the weight maps.

To further exanine the representational coding of overt and covert orienting in the FPN, we estimated and compared the contribution of overt/covert-preferred voxels and their joint contribution. The two extremes of continuums of the possible relationship would lead to distinct predictions. For a completely dependent relationship, a successful overt versus covert classification would be only achieved by combining overt- and covert-preferred voxels, but could not be achieved by each type of voxel solely. In contrast, for a completely independent relationship, a successful overt versus covert classification would be achieved by either overt- and covert-preferred voxels solely. Further, if a successful overt versus covert classification could be achieved by either type of voxel solely and combining the two types of voxels could significantly enhance the classification accuracy, it would be supported by a joint representational space comprised by interdependent voxels with different preferences, or supported by an increased amount of information conveyed by two independent types of voxels. In this analysis, to test the contribution of one type of voxel solely, we set the weights of all the voxels for the other type response bias (e.g., overt

preferred voxels with n_{covert} voxels) to zeros, and then applied this weight vector to predict the targets of 20% of trials randomly selected from the full data set of each participant. The comparable reference performance of the prediction in which voxels with both types of voxels combined was estimated by randomly selecting the equal number of weights (e.g., n_{overt}) from both overt- and covert-preferred voxels (e.g., set the weights of n_{covert} voxels into zeros, regardless of the sign of weight). The distributions of the empirical prediction performance were estimated by 1000 permutations, and the reference performance was estimated by another 1000 permutations. The mean performance of single type weight and the mean performance of reference prediction were computed across these permutations for each participant. At the group level, paired t-test was conducted to compare the single type performance to the reference performance. A paired t-test was also conducted to compare the empirical performance to the chance level.

To test the generalizability of the decoding across participants, cross-subject classification was performed, in which one participant's data set was used as the training set and another participant's data set was used as the testing set. The chance level performance was estimated for each pair of participants as the average performance of the 1000 permutations in which targets in the testing set were randomly shuffled. The mean performance of the 272 cross-subject classification was compared to the chance level performance as a paired t-test (one-tailed).

To test the generalizability of the decoding of overt and covert orienting across endogenous and exogeneous cueing, we conducted a cross-cueing-classification analysis, which used the all trials with one type of cueing (e.g., exogeneous) as the training set and trials with the other type of cueing (e.g., endogenous) as the testing set. Performance of the endogenous-to-exogeneous and exogeneous-to-endogenous classifications were estimated separately. Chance level performance of each cross-cueing classification was computed as the mean across 1000 permutations in which the target classes in the testing set were randomly shuffled. Paired t-tests were conducted to compared the performance of each cross-cueing classification to the corresponding chance level performance as the reference.

2.11. Characterizing the topological organization of the weight maps

Each participant's mean weight map as the average across all permutations in the above overt versus covert MVPA was further decomposed into overt- and covert-preferred clusters for each region of the FPN, defined as areas of voxels with positive weights surrounding local maxima and areas of voxels with negative weights surrounding local minima, respectively. The decomposition was based on Morse theory (Milnor, 1963) to identify topologically critical structures from a scalar function (i.e., a weight map within the FEF or IPS). In particular, it viewed the weight map as a terrain function and extracted its landscape features such as basins (areas surrounding local minima) and mountains (areas surrounding local maxima). The weight map was first decomposed into a covert-preferred domain comprised of all voxels with positive weights and an overt-preferred domain comprised of all voxels with negative weights. Then the overt-preferred domain was also decomposed into clusters, each of which is a Morse stable manifold of a local minimum (a basin with a unique local minimum), while the covert-preferred domain was further decomposed into

clusters, each of which is a Morse unstable manifold of a local maximum (a mountain with a unique local maximum). More details of the Morse decomposition can be found in Supplementary Methods and the implication of this method is introduced in Hu et al. (2021).The procedure of the decomposition was illustrated in Supplementary Fig. 1. Numbers of clusters were counted and the volume of each cluster was computed as the number of voxels in the cluster multiplying the voxel size ($2 \times 2 \times 2 = 8$ mm^3), and its isotropic size was computed as the cube root of the volume.

This decomposition approach characterized the clustering tendency of the weight maps, which considered the topological distribution of the weights in the space, which is not directly comparable to conventional clustering approaches such as K-means that mainly considers the geometric distribution of the weights. Clustering tendency of the weight maps was compared to the null distribution, which was estimated by performing Morse decomposition on each subject-level weight map generated by the permutation used to estimate the null distribution of classification performance and amplitude of the weights. The noise covariance across space and factors related to vascularization in these maps were consistent with those in the corresponding empirical maps. Pair-wise t-test was conducted to compared the empirical cluster size to the estimated chance level. Larger averaged cluster size indicates higher clustering tendency in the map.

Classic spatial statistics, i.e., the G and K functions (Besag and Green, 1993; Loosmore and Ford, 2006), were used to characterize the relative spatial arrangement of the overt- and covert-preferred clusters, i.e., an interlaced property. More details of the spatial statistics can be found in Supplementary Methods and Supplementary Figure 2.

3. Results

3.1. Eye-tracking and behavioral performance

Eye movements were successfully located to the cued locations, i.e., one of the eight peripheral circles in each trial, in the overt condition and were located around the central fixation in the covert condition (Fig. 2a). Distance of eye movement in each condition is shown in Fig. 2b and Supplementary Table 1. The main effect of Orienting (overt vs. covert) was significant, $F_{1, 16} = 898.80$, $p < .001$, $\eta_p^2 = .98$, with greater mean visual angle in the overt condition (Mean ± SD: 8.95 ± 0.21°) than in the covert condition (0.79 ± 0.10°). The main effect of Cueing (endogenous vs. exogenous) was not significant, $F_{1, 16} < 1$ (endogenous: 4.86 ± 0.09°, exogenous: 4.87 ± 0.10°), nor was the Orienting by Cueing interaction, $F_{1, 16} = 3.38$, $p = .085$, $\eta_p^2 = .17$. These findings indicate the distance of eye movement was driven by the type of orienting, and was not significantly impacted by the endogenous vs. exogenous cueing, which validated the manipulations of overt versus covert orienting in our task.

The mean behavioral accuracy was above 95% in all conditions (Fig. 2c and Supplementary Table 2), indicating that participants understood the task and followed the instructions to make responses as accurate as possible. Reaction time (RT) in each condition is shown in Fig. 2d and Supplementary Table 2. The main effect of Orienting was significant, $F_{1, 16} = 21.11$, $p < .001$, $\eta_p^2 = .57$, with a shorter mean RT in the overt condition (536.1 ± 19.9 ms)

compared to the covert condition (606.2 ± 20.3 ms). The main effect of Cueing was also significant, $F_{1, 16} = 6.54$, $p = .021$, $\eta_p^2 = .29$, with a prolonged mean RT in the endogenous condition (579.6 ± 20.2 ms) compared to the exogenous condition (562.7 ± 17.4 ms). The Orienting by Cueing interaction was not significant, $F_{1, 16} = 1.54$, $p = .23$, $\eta_p^2 = .09$. These results indicate that covert orienting is more difficult than overt orienting, and the exogenous cueing is more effective than endogenous cueing.

3.2. Involvement of the whole brain and the FPN in overt and covert orienting of attention

The contrast of overt-minus-fixation-baseline revealed significant bilateral activation in regions of the FPN, including frontal regions of the supplementary motor area (SMA) extending to the anterior cingulate cortex (ACC) and the superior and middle frontal gyri extending to the precentral gyrus, as well as in the parietal regions of the IPS extending to the superior parietal lobule (SPL). This contrast also revealed significant bilateral activation in visual areas (including the calcarine cortex, middle and inferior occipital gyri, fusiform gyrus, and middle temporal gyrus), and subcortical regions of thalamus, putamen, superior colliculus, pulvinar, dorsal and ventral part of cerebellum, and vermis (Fig. 3a and Supplementary Table 3). The contrast of covert-minus-fixation-baseline revealed significant bilateral activation in regions of the FPN, and in the anterior insular cortex (AIC), visual areas (including middle and inferior occipital gyri, fusiform gyrus, and middle temporal gyrus), and subcortical regions of thalamus, putamen, superior colliculus, dorsal and ventral part of cerebellum, and vermis (Fig. 3b and Supplementary Table 4). The conjunction between these two contrasts revealed significant bilateral activation in the FPN, visual areas (including middle and inferior occipital gyri, fusiform gyrus, and middle temporal gyrus), the thalamus, and the dorsal and ventral parts of cerebellum, as well as unilateral activation in the left superior colliculus (regions in violet in Fig. 3c and Supplementary Table 5). Disjunction analysis showed that the overt condition was specifically associated with bilateral activation in the primary visual areas (calcarine cortex and lingual gyrus) and the pulvinar, and that the covert condition was specifically associated with bilateral activation in the ACC, the AIC, the anterior portion of the thalamus, as well as unilateral activation in the right superior temporal gyrus and the right superior colliculus (Fig. 3c and Supplementary Table 6). The contrast of overt > covert revealed a significant activation in the left and right calcarine cortex, while the contrast of covert > overt did not reveal significant activation in any region (Fig. 3d and Supplementary Table 6). Similar results were found by using the conventional GLM (see Supplementary materials and Supplementary Fig. 3 for details).

The ROIs of the FPN were comprised of a frontal FEF-centered ROI and a parietal ROI that included mainly the IPS, both defined as the regions that showed significant activation in the conjunction between the contrasts of covert-minus-fixation-baseline and overt-minus-fixation-baseline. Specifically, the ROI of the FEF (highlighted as white dashed contours in Fig. 3) was defined as the frontal areas located in the region around the intersection of superior frontal gyrus and middle frontal gyrus, and extending to the SMA and the precentral gyrus. The ROI of the IPS (highlighted as green dashed contours in Fig. 3) was defined as the parietal areas including the anterior, ventral, medial, lateral, and caudal portions of the IPS, and the SPL. Comparison between activation in the overt and covert conditions did not show any significant difference under the thresholds of FWE corrected

$p < .05$ with small volume correction restricting the comparison within the FPN (Fig. 3d). Averaged regional activation of the FEF and the IPS are illustrated in Supplementary Fig. 4, with a significantly greater activation in the covert conditions than in the overt conditions revealed only in the right FEF. Each participant's voxel-wise activation in the FPN for the overt versus covert contrast estimated based on unsmoothed data is illustrated in Supplementary Fig. 5.

3.3. MVPA classification performance of overt versus covert orienting based on activation of the FPN

The classification of overt versus covert orienting using linear SVM reached an accuracy of 85.8 ± 4.9%, 85.8 ± 4.5%, and 89.9 ± 4.6% by patterns of voxel-wise activation in the ROIs of the FEF, the IPS, and the FPN (i.e., FEF and IPS combined), respectively (Fig. 4a). The classification accuracy based on the FPN was significantly higher than the accuracy based on the FEF alone, $t_{16} = 10.05$, $p < .001$ and the IPS alone, $t_{16} = 12.39$, $p < .001$, while the difference between the FEF and IPS was not significant, $t_{16} < 1$. Spatial smoothing using a FWHM as 8 × 8 × 8 mm Gaussian kernel resulted in a significant decrease in classification accuracy for each ROI (FEF: 75.1 ± 5.7%, IPS: 76.4 ± 3.9%, FPN: 80.7 ± 5.1%; all ps < .001). Precision, recall, and F1 score of these classifications are reported in Supplementary Table 7, which did not show any bias to either overt or covert condition. All of these measures were significantly higher than chance level of 50.4 ± 0.6% (ps < .001). Accuracy of the control analysis considering the block structure was also significantly higher than chance level for each ROI (FEF: 59.7 ± 7.0% > 50.0 ± 1.9%, $t_{16} = 5.14$, $p < .0001$; IPS: 55.1 ± 4.1% > 50.1 ± 1.5%, $t_{16} = 4.72$, $p = .0001$), indicating the classifications were not biased by the trial sampling method.

Accuracy of the cross-subject classification, i.e., training the overt-versus-covert classifier based on all data from one participant and testing its performance on data from other participants, was 55.0 ± 0.7%, 54.1 ± 0.8%, and 55.0 ± 0.7% for the FEF, IPS, and FPN, respectively on average, which was close to but significantly higher than the chance level (all ps < .001; Fig. 4b and Supplementary Table 8). Accuracy of the cross-cueing classifications, i.e., training the overt-versus-covert classifier based on trials in the one cueing condition and testing its performance on the trials in the other condition (endogenous-to-exogenous and exogenous-to-endogenous cross-classifications), ranged from 66% to 72%, were significantly above the chance level (ps < .001) and did not show any bias to either overt or covert condition (Fig. 4c and Supplementary Table 9).

SVM weight maps of the overt-versus-covert classification based on activation of voxels in the FEF, IPS, and FPN were illustrated for two participants in Fig. 5a–5c (see Supplementary Fig. 6–8 for the weight maps for the other participants). Most of voxels showed weights significantly different from the null distribution for both FEF and IPS, while only a small proportion of voxels showed univariate voxel-wise activation significantly different from zero (see Supplementary Table 10 for details). For the group-average of the weight maps across all participants, no voxels in the FEF and the IPS cluster showed significant difference from the null distribution.

Both voxels with positive and negative SVM weight values revealed positive beta values (activation) in both overt and covert conditions (Fig. 5d). The overt condition was associated with a pattern that the voxels with positive weight values showed lower activation (lower beta values and negative z values) than the voxels with negative weight values (higher beta values and positive z values), while the covert condition showed a reversed pattern (Fig. 5e). The univariate activation could account for 38.5 ± 10.6% of variance of the weights (r = .615 ± .086) for the FEF, and 38.6 ± 11.7% variance of the weights (r = .615 ±. 094) for the and IPS, respectively. Therefore, voxels with negative and positive weights can be considered as overt- and covert-preferred voxels, respectively.

Classifications by activation of overt-preferred voxels alone reached an accuracy of 62.0 ± 6.5% for the FEF and 57.9 ± 3.7% for the IPS, while accuracy of the classification by activation in the covert-preferred voxels was 57.8 ± 5.1% for the FEF and 56.9 ± 3.2% for the IPS, (Fig. 6). These accuracies were slightly but significantly higher than the chance level (ps < .001). Combining the two types of voxels when controlling the total number of voxels led to a significant superadditive increase of classification accuracies (FEF: 96.1 ± 2.4%, IPS: 88.1 ± 5.9%; all ps < .001). Precision, recall, and F1 score of these classifications are reported in Supplementary Table 11, which did not show any bias to either overt or covert condition.

3.4. Topological property of the spatial distribution of the overt- and covert-preferred voxels

The analysis of the topological properties of the spatial distribution of the overt- and covert-preferred clusters of voxels revealed that the two types of clusters were interlaced with an average cluster size of 14.3 ± 3.1 voxels for the FEF and 14.0 ± 2.3 voxels for the IPS (Supplementary Table 12), which was significantly smaller than the chance level cluster size (FEF: 98.8 ± 16.6 voxels, IPS: 83.2 ± 8.1 voxels). This finding indicates that the clustering tendency for voxels with the same preference in these ROIs was significantly different from the clustering tendency of randomly distributed noise. Specifically, based on the topological distribution of the overt- and covert-preferred voxels in space, areas within each FPN region were decomposed into about 500 to 600 clusters based on the discrete version of Morse theory. Nearly half of these were overt-preferred clusters, i.e., areas of voxels with negative weights surrounding a local minimum, and the other half were covert-preferred clusters, i.e., areas of voxels with positive weights surrounding a local maximum (Fig. 7a and 7b). Each cluster was comprised of 10 to 20 voxels corresponding to a 4 to 5 mm isotropic volume. Spatial statistical analysis showed that the overt- and covert-preferred voxels within each region of the FPN were organized as distinct clusters that distributed as an interlaced pattern in the same space. See Supplementary Materials and Supplementary Fig. 9 for the results of the specific analysis of the topological distribution.

4. Discussion

This study demonstrated an interdependent relationship between overt and covert orienting. The common activation of the FPN in both overt and covert orienting of attention found in this study and previous fMRI studies (Beauchamp et al., 2001; Corbetta, 1998; Corbetta et

al., 1998; De Haan et al., 2008; Fairhall et al., 2009; Gitelman et al., 2002; Grosbras et al., 2005; Nobre et al., 2000; Nobre et al., 1997) supports some dependence of these two types of orienting. In contrast, the distinct underlying representational coding of orienting revealed by the significant predictive power of the multivariate patterns of activation in the regions of the FPN supports independence of overt and covert orienting, consistent with findings from single-cell recording studies in monkeys (Bruce and Goldberg, 1985; Bruce et al., 1985; Cohen et al., 2009; Sato and Schall, 2003; Schall, 1991). Importantly, the joint classification power of overt- and covert-preferred clusters of voxels, the superadditivity, indicates an interdependent relationship. That is, each type of cluster could predict the orienting type slightly but significantly better than chance level, and these two types of clusters together led to a significant superadditive increase in prediction accuracy, with the amplitude of the increase being greater than the sum of the accuracy increases (compared to chance level) by each type of clusters. Joint involvement of the two types of clusters with different preference may convey unique information for the representation of overt and covert orienting, beyond the additive effect of the information conveyed by each type of clusters. Even though overt and covert orienting could be solely implemented by an independent representation in its corresponding type of cluster, an interdependent representation that involves both types of clusters leads to more reliable coding of orienting.

Voxel-wise multivariate pattern of activation in the FPN is likely associated with the underlying neuronal-level mechanism. The spatial resolution of voxel-wise activation observed in fMRI studies is much lower than the scale of neuronal populations. However, the spatial distribution of neuronal populations impacts the relative magnitude difference across voxels (i.e., the pattern of activation) within a brain region demonstrated in previous studies on the representational coding of stimulus orientation in the primary visual cortex (Alink et al., 2013; Boynton, 2005; Haynes and Rees, 2005; Kamitani and Tong, 2005). These studies revealed that millimeter-level activation patterns in the primary visual cortex arise from random spatial irregularities in the map of below-millimeter level orientation columns. Specifically, activation in each individual voxel emerges from a combination of activity of all neural populations inside this voxel. The inhomogeneity of the spatial distribution of populations of neurons across voxels leads to a mosaic-like spatial distribution of voxel-wise activation with idiosyncratic biases in individual voxels (Kamitani and Tong, 2005; Swisher et al., 2010; Tong and Pratte, 2012). Similar to the encoding of stimulus orientation in the primary visual cortex, there is a continuum of visual-movement functions among neurons within the FEF (Moore et al., 2012), and attention selection and eye movement control are implemented by selectively activating and suppressing the populations of visual and motor neurons in the FEF (Thompson et al., 2005). Therefore, if there is random variability in the spatial distribution of the neurons with visual and motor preferences, the proportion of different populations contributing to the activity of each individual voxel may lead to a bias in the activity. Overt orienting would be associated with a pattern of higher activation in voxels containing more motor-preferred neurons (overt-preferred voxels) than in voxels containing more visual-preferred neurons (covert-preferred voxels), while covert orienting would be associated with the reverse pattern.

There are several possible alternative explanations for the classification power of the activation in the FPN on the type of orienting. For example, overt and covert conditions

differed in task difficulty. In this study, selective activation in the overt condition was observed in the primary visual cortex, likely reflecting foveation of the target in this condition that is typically associated with enhanced activity in visual cortex (Corbetta et al., 1998). In contrast, selective activation in the covert condition, which was more difficult, was observed in the ACC and AIC that are typically associated with task difficulty indicated by prolonged RT as in literature (e.g., Mulert et al., 2003; Naito et al., 2000; Yarkoni et al., 2009). However, these selective responses were not observed in the FPN. These results suggest that task difficulty did not significantly contribute to the classification of the type of orienting by the activation in the FPN.

The topological property of the pattern of distinct and interlaced clusters of overt- and covert-preferred voxels in regions of FPN suggests a fine-scale representational coding of orienting within each region of the FPN. The representational coding of orienting may be organized as a fine-scale pattern within each anatomical region with multiple overt- and covert-preferred subdivisions, which is in contrast to a coarse-scale pattern driven by mean regional activation in different anatomical regions (Swisher et al., 2010; Tong and Pratte, 2012). The clustering of voxels found in the weight maps was organized as millimeter-level isotropic clusters for each region, rather than distinct patterns of regional activation across regions of the FPN. This suggests that overt and covert orienting are encoded by a fine-scale representation in the FPN, rather than a clear segregation by anatomical landmarks forming different regions or sub-regions. The finding of reduced classification accuracy by spatially smoothing the images further demonstrated the existence of fine-scale representation that would be detrimentally impacted by reduction of spatial resolution (Op de Beeck, 2010). This fine-scale representational coding echoes findings from single cell recording studies in monkeys showing that visual, motor, and visuo-motor neurons are mixed in the FEF (Bruce and Goldberg, 1985; Bruce et al., 1985; Schall, 1991).

Although the anatomical properties (e.g., layer, morphological cell type) of neuronal populations in the FPN are still poorly understood (Squire et al., 2012), the distinct and interlaced clusters revealed by MVPA in this study may provide insight into the within-region topological distribution of the neuronal populations. Although intra-region fine-scale activation pattern may reflect the spatial organization of underlying neuronal populations, the pattern has rarely been characterized due to the lack of a corresponding methodology. The Morse decomposition together with spatial statistics provides an approach to quantify the clustering tendency of voxels with different response preferences in the pattern. High clustering tendency may lead to functional segregation as different sub-regions, which may be associated with an independence of associated functions. In contrast, the interlaced distribution of clusters with different preferences within the same anatomical region of the FPN likely facilitates the coordination of attention orienting and attention guided eye movement via microstructural neural circuits, which may be more efficient than via macrostructural circuit between distinct anatomical regions. The use of unsmoothed images which were acquired using multiband sequence with a relatively high spatial resolution in this study may facilitate the detection of the fine-scale representation within the FPN (see Supplementary Discussion for more information). It is worth noting that the absolute size of isotropic clusters cannot be treated as an estimate of the size of neuronal population, because although the BOLD signal and electrical signal are associated, they are also different in

many aspects. Spatial smoothing in image preprocessing steps (e.g., normalization) and the thresholding parameter in the Morse decomposition may also impact the absolute size of isotropic clusters. In addition, the accuracy of the classification based on the combination of the FEF and IPS was slightly but significantly higher than the classification based on FEF or IPS alone. This indicates that the fine-scale representations of orienting within these two regions are largely redundant but with some unique contribution. However, the increased of number of voxels in the combination feature set might also have contributed to the enhanced classification accuracy.

Although the patterns of activation in the FPN were comprised of two types of clusters with different response biases (one cluster type is activated more than the other type of cluster), their common activation in both overt and covert conditions (the above baseline activation of both types of clusters) represents the general involvement of FPN in orienting. This finding provides further support for an interdependent mechanism of overt and covert orienting in the FPN. That is, activation pattern of the cluster with each type of cluster conveys some information for whether the corresponding type of orienting is executing, as the independent aspect of the relationship. The joint pattern comprised by the two types of clusters further provides additional information of the orienting type, as the dependent aspect of the relationship. Therefore, the relationship of overt and covert orienting is in between these two extremes, i.e., interdependent. The two types of clusters are not dissociable when only examining the involvement of the FPN in two types of orienting as in previous studies (Beauchamp et al., 2001; Corbetta et al., 1998; De Haan et al., 2008; Grosbras et al., 2005; Nobre et al., 1997). Univariate (voxel-wise) comparison employed in previous studies to disassociate the two types of orienting reported either no significant difference in the FPN (De Haan et al., 2008; Fairhall et al., 2009), or an impact on mean regional activation associated with the condition with a higher task difficulty (Corbetta et al., 1998; Nobre et al., 2000; Nobre et al., 1997). Although univariate analysis is powerful in examination of impact on mean regional activation, it is not sensitive to the fine scale patterns of activation (Davis et al., 2014). In this study, voxels revealing significant difference in activation between overt and covert conditions were barely observed with subject-level univariate analysis. In addition, because of the large cross-subject variability in the spatial distribution of these clusters as demonstrated in this study, it is almost impossible to reveal common clusters at group level in the univariate analysis. The spatial smoothing and cluster-level extent threshold applied in the univariate analysis may further eliminate the possibility to detect clusters of voxels with significant overt versus. covert difference shared across participants in the current study as well as in previous studies. The low accuracy of cross-subject decoding and the large cross-subject variability in the weight maps indicate that there is minimal overlap in the topological distribution of neuronal populations in the FPN across individuals.

The successful cross-cueing-decoding (i.e., the endogenous-to-exogeneous and exogeneous-to-endogenous cross-cueing-classifications) suggests that the representational coding of overt and covert orienting in the FPN is a high-level encoding mechanism that is independent of how attention is summoned by the cue. It has been proposed that attention guided eye movement and attentional orienting are only closely related for exogenous cueing towards peripheral events, but not for endogenous cueing (Casteau and Smith,

2019; Reuter-Lorenz and Fendrich, 1992; Smith et al., 2012). In this way, eye movement and attention would be functionally related for the processing of peripheral events rather than have intrinsic physiological relationship (Posner, 1980). However, the successful cross-cueing-decoding together with the non-significant orienting by cueing interaction in behavioral performance found in this study do not support this account. Instead, this finding provides evidence for a general representation of orienting that is not specific to endogenous or exogenous orienting.

This study demonstrates that eye movements and covert attention are encoded by fine-scale, interdependent, interlaced functional clusters in the FPN. Intermingling of motor and attentional functions has been observed in FEF-homologue areas in non-human primates as described above as well as in the arcopallilal gaze field of the barn owl (Winkowski and Knudsen, 2006; Winkowski and Knudsen, 2008). The interdependent fine scale representational pattern of closely associated processes in the brain may therefore reflect a generalizable principle of functional organization for orienting in the brain across species (Squire et al., 2012). Whether this organizational principle applies to other types of closely associated functions remains to be investigated.

Supplementary Material

Refer to Web version on PubMed Central for supplementary material.

Acknowledgements

We thank Mr. Alexander Dufford for assistance with data collection, Dr. Hongtao Chen for the help in exploration of the smoothing parameters, Mr. Fan Wang, Mr. Songzhu Zheng, and Mr. Xiaoling Hu for the help on the implication of topological analysis. We specifically thank Dr. Michael I. Posner for his guidance trough all stages of this project. Research reported in this publication was supported by National Institute of Mental Health (NIMH) of the National Institutes of Health (NIH R01 MH094305) and the grant of National Science Foundation (NSF IIS 1718802).

FEF Data and Code Availability Statement

All of the individual-level behavioral and imaging data used in this study cannot be shared because of the lack of approval by the IRBs for a data-sharing agreement. Group-level result images are available in the NeuroVault collection of this study (https://neurovault.org/collections/12519/). E-prime scripts for stimuli presentation and MATLAB and Python scripts for image preprocessing, fMRI modeling, and Morse decomposition are available in the GitHub repository of this study (https://github.com/TingtingWu222/COAT).

References

Alink A, Krugliak A, Walther A, Kriegeskorte N, 2013. fMRI orientation decoding in V1 does not require global maps or globally coherent orientation stimuli. Front. Psychol 4, 493. [PubMed: 23964251]

Awh E, Armstrong KM, Moore T, 2006. Visual and oculomotor selection: links, causes and implications for spatial attention. Trends Cogn. Sci 10, 124–130. [PubMed: 16469523]

Beauchamp MS, Petit L, Ellmore TM, Ingeholm J, Haxby JV, 2001. A parametric fMRI study of overt and covert shifts of visuospatial attention. Neuroimage 14, 310–321. [PubMed: 11467905]

Belopolsky AV, Theeuwes J, 2012. Updating the premotor theory: the allocation of attention is not always accompanied by saccade preparation. J. Exp. Psychol. Hum. Percept. Perform 38, 902–914. [PubMed: 22686694]

Berger C, Winkels M, Lischke A, Höppner J, 2012. GazeAlyze: a MATLAB toolbox for the analysis of eye movement data. Behav. Res. Method 44, 404–419.

Besag J, Green PJ, 1993. Spatial statistics and Bayesian computation. J. R. Stat. Soc.Series B (Methodol.) 55, 25–37.

Boynton GM, 2005. Imaging orientation selectivity: decoding conscious perception in V1. Nat. Neurosci 8, 541–542. [PubMed: 15856054]

Bruce CJ, Goldberg ME, 1985. Primate frontal eye fields. I. Single neurons discharging before saccades. J. Neurophysiol 53, 603–635. [PubMed: 3981231]

Bruce CJ, Goldberg ME, Bushnell MC, Stanton GB, 1985. Primate frontal eye fields. II. Physiological and anatomical correlates of electrically evoked eye movements. J. Neurophysiol 54, 714–734. [PubMed: 4045546]

Casteau S, Smith DT, 2019. Associations and Dissociations between Oculomotor Readiness and Covert Attention. Vision (Basel) 3.

Choi JM, Padmala S, Pessoa L, 2012. Impact of state anxiety on the interaction between threat monitoring and cognition. Neuroimage 59, 1912–1923. [PubMed: 21939773]

Cohen JY, Heitz RP, Woodman GF, Schall JD, 2009. Frontal eye field activity before form visual search errors. J. Vision 9, 759.

Corbetta M, 1998. Frontoparietal cortical networks for directing attention and the eye to visual locations: Identical, independent, or overlapping neural systems? In: Proceedings of the National Academy of Sciences of the United States of America, 95, pp. 831–838. [PubMed: 9448248]

Corbetta M, Akbudak E, Conturo TE, Snyder AZ, Ollinger JM, Drury HA, Linen-weber MR, Petersen SE, Raichle ME, Van Essen DC, 1998. A common network of functional areas for attention and eye movements. Neuron 21, 761–773. [PubMed: 9808463]

Cortes C, Vapnik V, 1995. Support-vector networks. Machine learning 20, 273–297.

Davis T, LaRocque KF, Mumford JA, Norman KA, Wagner AD, Poldrack RA, 2014. What do differences between multi-voxel and univariate analysis mean? How subject-, voxel-, and trial-level variance impact fMRI analysis. Neuroimage 97, 271–283. [PubMed: 24768930]

De Haan B, Morgan PS, Rorden C, 2008. Covert orienting of attention and overt eye movements activate identical brain regions. Brain Res. 1204, 102–111. [PubMed: 18329633]

Delgado-Friedrichs O, Robins V, Sheppard A, 2015. Skeletonization and Partitioning of Digital Images Using Discrete Morse Theory. IEEE Trans. Pattern Anal. Mach. Intell 37, 654–666. [PubMed: 26353267]

Diggle PJ, Besag J, Gleaves JT, 1976. Statistical analysis of spatial point patterns by means of distance methods. Biometrics 659–667.

Fairhall SL, Indovina I, Driver J, Macaluso E, 2009. The brain network underlying serial visual search: comparing overt and covert spatial orienting, for activations and for effective connectivity. Cereb. Cortex 19, 2946–2958. [PubMed: 19395524]

Faul F, Erdfelder E, Buchner A, Lang AG, 2009. Statistical power analyses using G*Power 3.1: tests for correlation and regression analyses. Behav. Res. Methods 41, 1149–1160. [PubMed: 19897823]

Forman R, 2002. A user's guide to discrete Morse theory. Séminaire Lotharingien de Combinatoire [electronic only] 48 (B48c), 35 p., electronic only-B48c, 35 p., electronic only.

Friston KJ, Josephs O, Rees G, Turner R, 1998. Nonlinear event-related responses in fMRI. Magn. Reson. Med 39, 41–52. [PubMed: 9438436]

Friston KJ, Worsley KJ, Frackowiak RS, Mazziotta JC, Evans AC, 1994. Assessing the significance of focal activations using their spatial extent. Hum. Brain Mapp 1, 210–220. [PubMed: 24578041]

Gardumi A, Ivanov D, Hausfeld L, Valente G, Formisano E, Uludag K, 2016. The effect of spatial resolution on decoding accuracy in fMRI multivariate pattern analysis. Neuroimage 132, 32–42. [PubMed: 26899782]

Gitelman DR, Parrish TB, Friston KJ, Mesulam MM, 2002. Functional anatomy of visual search: regional segregations within the frontal eye fields and effective connectivity of the superior colliculus. Neuroimage 15, 970–982. [PubMed: 11906237]

Glasser MF, Sotiropoulos SN, Wilson JA, Coalson TS, Fischl B, Andersson JL, Xu J, Jbabdi S, Webster M, Polimeni JR, 2013. The minimal preprocessing pipelines for the Human Connectome Project. Neuroimage 80, 105–124. [PubMed: 23668970]

Gómez-Rubio V, 2016. Spatial Point Patterns: Methodology and Applications with R. J. Stat. Softw 75.

Grosbras MH, Laird AR, Paus T, 2005. Cortical regions involved in eye movements, shifts of attention, and gaze perception. Hum. Brain Mapp 25, 140–154. [PubMed: 15846814]

Haxby JV, 2012. Multivariate pattern analysis of fMRI: the early beginnings. Neuroimage 62, 852–855. [PubMed: 22425670]

Haxby JV, Gobbini MI, Furey ML, Ishai A, Schouten JL, Pietrini P, 2001. Distributed and overlapping representations of faces and objects in ventral temporal cortex. Science 293, 2425–2430. [PubMed: 11577229]

Haynes J-D, Rees G, 2005. Predicting the orientation of invisible stimuli from activity in human primary visual cortex. Nat. Neurosci 8, 686–691. [PubMed: 15852013]

Hu X, Wang Y, Li F, Samaras D, Chen C, 2021. Topology-Aware Segmentation Using Discrete Morse Theory. Ninth International Conference on Learning Representations (ICLR), Virtual Only.

Hunt AR, Kingstone A, 2003. Inhibition of return: Dissociating attentional and oculomotor components. J. Exp. Psychol. Hum. Percept. Perform 29, 1068–1074. [PubMed: 14585023]

Jonikaitis D, Moore T, 2019. The interdependence of attention, working memory and gaze control: behavior and neural circuitry. Curr. Opin. Psychol 29, 126–134. [PubMed: 30825836]

Kamitani Y, Tong F, 2005. Decoding the visual and subjective contents of the human brain. Nat. Neurosci 8, 679–685. [PubMed: 15852014]

Kinnison J, Padmala S, Choi J-M, Pessoa L, 2012. Network analysis reveals increased integration during emotional and motivational processing. J. Neurosci 32, 8361–8372. [PubMed: 22699916]

Loosmore NB, Ford ED, 2006. Statistical inference using the G or K point pattern spatial statistics. Ecology 87, 1925–1931. [PubMed: 16937629]

Mandelkow H, de Zwart JA, Duyn JH, 2017. Effects of spatial fMRI resolution on the classification of naturalistic movies. Neuroimage 162, 45–55. [PubMed: 28842385]

Milnor J, 1963. Morse Theory. Princeton University Press, Princeton, NJ.

Misaki M, Kim Y, Bandettini PA, Kriegeskorte N, 2010. Comparison of multivariate classifiers and response normalizations for pattern-information fMRI. Neuroimage 53, 103–118. [PubMed: 20580933]

Misaki M, Luh WM, Bandettini PA, 2013. The effect of spatial smoothing on fMRI decoding of columnar-level organization with linear support vector machine. J. Neurosci. Methods 212, 355–361. [PubMed: 23174092]

Moore T, Armstrong KM, Fallah M, 2003. Visuomotor Origins of Review Covert Spatial Attention. Neuron 40, 671–683. [PubMed: 14622573]

Moore T, Burrows B, Armstrong KM, Schafer RJ, Chang MH, 2012. Neural circuits controlling visual attention. Cognit. Neurosci. Atten 257–276.

Mulert C, Gallinat J, Dorn H, Herrmann WM, Winterer G, 2003. The relationship between reaction time, error rate and anterior cingulate cortex activity. Int. J. Psychophysiol 47, 175–183. [PubMed: 12568947]

Müller HJ, Rabbitt PM, 1989. Reflexive and voluntary orienting of visual attention: time course of activation and resistance to interruption. J. Exp. Psychol. Hum. Percept. Perform 15, 315. [PubMed: 2525601]

Naito E, Kinomura S, Geyer S, Kawashima R, Roland PE, Zilles K, 2000. Fast reaction to different sensory modalities activates common fields in the motor areas, but the anterior cingulate cortex is involved in the speed of reaction. J. Neurophysiol 83, 1701–1709. [PubMed: 10712490]

Nobre AC, Gitelman D, Dias E, Mesulam M, 2000. Covert visual spatial orienting and saccades: overlapping neural systems. Neuroimage 11, 210–216. [PubMed: 10694463]

Nobre AC, Sebestyen GN, Gitelman DR, Mesulam MM, Frackowiak R, Frith CD, 1997. Functional localization of the system for visuospatial attention using positron emission tomography. Brain J. Neurol 120, 515–533.

Norman KA, Polyn SM, Detre GJ, Haxby JV, 2006. Beyond mind-reading: multi- -voxel pattern analysis of fMRI data. Trends Cogn. Sci 10, 424–430. [PubMed: 16899397]

Oldfield RC, 1971. The assessment and analysis of handedness: the Edinburgh inventory. Neuropsychologia 9, 97–113. [PubMed: 5146491]

Op de Beeck HP, 2010. Against hyperacuity in brain reading: spatial smoothing does not hurt multivariate fMRI analyses? Neuroimage 49, 1943–1948. [PubMed: 19285144]

Padmala S, Pessoa L, 2011. Reward reduces conflict by enhancing attentional control and biasing visual cortical processing. J. Cogn. Neurosci 23, 3419–3432. [PubMed: 21452938]

Peelen MV, Downing PE, 2007. Using multi-voxel pattern analysis of fMRI data to interpret overlapping functional activations. Trends Cogn. Sci 11, 4–5. [PubMed: 17129747]

Peelen MV, Wiggett AJ, Downing PE, 2006. Patterns of fMRI activity dissociate overlapping functional brain areas that respond to biological motion. Neuron 49, 815–822. [PubMed: 16543130]

Petersen SE, Posner MI, 2012. The attention system of the human brain: 20 years after. Annu. Rev. Neurosci 35, 73–89. [PubMed: 22524787]

Posner MI, 1980. Orienting of Attention. Q. J. Exp. Psychol 32, 3–25. [PubMed: 7367577]

Posner MI, 2016. Orienting of attention: Then and now. Q. J. Exp. Psychol 69, 1864–1875.

Posner MI, Petersen SE, 1990. The attention system of the human brain. Annu. Rev. Neurosci 13, 25–42. [PubMed: 2183676]

Posner MI, Rafal RD, Choate LS, Vaughan J, 1985. Inhibition of return: Neural basis and function. Cognit. Neuropsychol 2, 211–228.

Ptak R, Schnider A, Fellrath J, 2017. The dorsal frontoparietal network: a core system for emulated action. Trends Cogn. Sci 21, 589–599. [PubMed: 28578977]

Reuter-Lorenz PA, Fendrich R, 1992. Oculomotor readiness and covert orienting: Differences between central and peripheral precues. Percep. Psychophys 52, 336–344.

Rissman J, Gazzaley A, D'esposito M, 2004. Measuring functional connectivity during distinct stages of a cognitive task. Neuroimage 23, 752–763. [PubMed: 15488425]

Rizzolatti G, Riggio L, Dascola I, Umiltá C, 1987. Reorienting attention across the horizontal and vertical meridians: evidence in favor of a premotor theory of attention. Neuropsychologia 25, 31–40. [PubMed: 3574648]

Rizzolatti G, Riggio L, Sheliga BM, 1994. Space and selective attention. Attention and performance XV 15, 231–265.

Sato TR, Schall JD, 2003. Effects of stimulus-response compatibility on neural selection in frontal eye field. Neuron 38, 637–648. [PubMed: 12765614]

Schall JD, 1991. Neuronal activity related to visually guided saccades in the frontal eye fields of rhesus monkeys: comparison with supplementary eye fields. J. Neurophysiol 66, 559–579. [PubMed: 1774586]

Schall JD, 2004. On the role of frontal eye field in guiding attention and saccades. Vision Res. 44, 1453–1467. [PubMed: 15066404]

Shulman GL, Pope DL, Astafiev SV, McAvoy MP, Snyder AZ, Corbetta M, 2010. Right hemisphere dominance during spatial selective attention and target detection occurs outside the dorsal frontoparietal network. J. Neurosci 30, 3640–3651. [PubMed: 20219998]

Smith DT, Schenk T, Rorden C, 2012. Saccade preparation is required for exogenous attention but not endogenous attention or IOR. J. Exp. Psychol. Hum. Percept. Perform 38, 1438. [PubMed: 22428677]

Spitzer R, Williams J, Gibbon M, First M, 1994. Structured Clinical Interview for DSM-IV (SCID-IV). American Psychiatric Press, Washington DC.

Squire RF, Steinmetz NA, Moore T, 2012. Frontal eye field. Scholarpedia 7, 5341.

Swisher JD, Gatenby JC, Gore JC, Wolfe BA, Moon CH, Kim SG, Tong F, 2010. Multiscale pattern analysis of orientation-selective activity in the primary visual cortex. J. Neurosci 30, 325–330. [PubMed: 20053913]

Szczepanski SM, Pinsk MA, Douglas MM, Kastner S, Saalmann YB, 2013. Functional and structural architecture of the human dorsal frontoparietal attention network. Proc. Natl. Acad. Sci. U. S. A 110, 15806–15811. [PubMed: 24019489]

Thompson KG, Biscoe KL, Sato TR, 2005. Neuronal basis of covert spatial attention in the frontal eye field. J. Neurosci 25, 9479–9487. [PubMed: 16221858]

Tong F, Pratte MS, 2012. Decoding patterns of human brain activity. Annu. Rev. Psychol 63, 483–509. [PubMed: 21943172]

Wechsler D, 2008. In: Wechsler adult intelligence scale–Fourth Edition (WAIS–IV), 22. NCS Pearson, San Antonio, TX, p. 1.

Winkowski DE, Knudsen EI, 2006. Top-down gain control of the auditory space map by gaze control circuitry in the barn owl. Nature 439, 336–339. [PubMed: 16421572]

Winkowski DE, Knudsen EI, 2008. Distinct mechanisms for top-down control of neural gain and sensitivity in the owl optic tectum. Neuron 60, 698–708. [PubMed: 19038225]

Wright RD, Ward LM, 2008. Orienting of attention. Oxford University Press.

Wu T, Dufford AJ, Egan LJ, Mackie M-A, Chen C, Yuan C, Chen C, Li X, Liu X, Hof PR, Fan J, 2018. Hick–Hyman Law is Mediated by the Cognitive Control Network in the Brain. Cereb. Cortex 28, 2267–2282. [PubMed: 28531252]

Xuan B, Mackie M-A, Spagna A, Wu T, Tian Y, Hof PR, Fan J, 2016. The activation of interactive attentional networks. Neuroimage 129, 308–319. [PubMed: 26794640]

Yarkoni T, Barch DM, Gray JR, Conturo TE, Braver TS, 2009. BOLD Correlates of Trial-by-Trial Reaction Time Variability in Gray and White Matter: A Multi-Study fMRI Analysis. PLoS One 4.

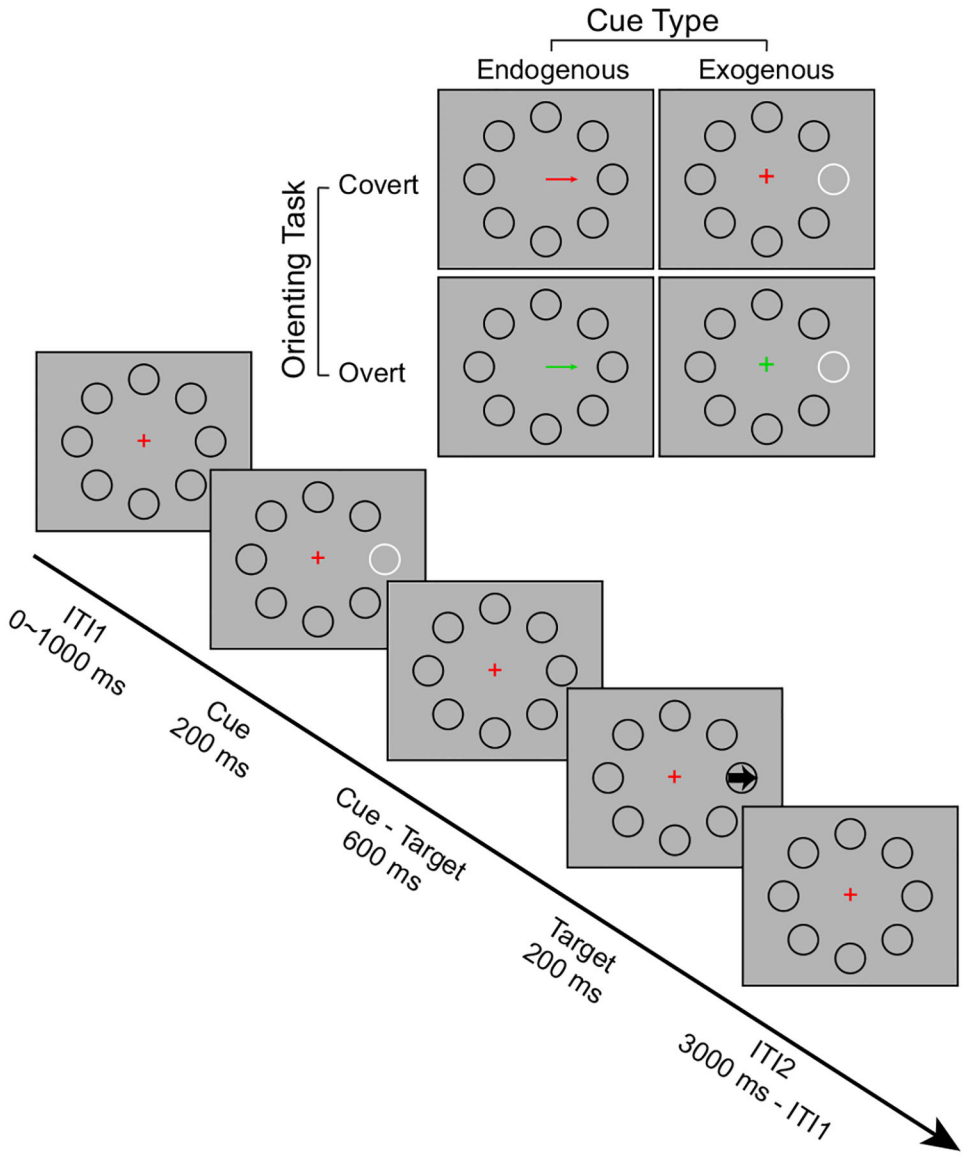

Figure 1.

Schematic of the overt and covert orienting tasks. Diagonal timeline: schematic of one trial in the covert orienting and exogenous cueing condition. In this task, the fixation cross and eight circles around the fixation were presented on the screen for the whole experiment. After a variable fixation period of inter-trial-interval (ITI1, 0–1000 ms), a cue appeared for 200 ms, followed by a cue-target interval of 600 ms. Participants were required to move eyes towards the cued-location after the onset of the cue if the central fixation was green (overt block), and to maintain central fixation during the entire block if the central fixation was red (covert block). A target arrow then appeared at the cued location and was presented for 200 ms, followed by another varied fixation period (ITI2, 3000 ms – ITI1). Participants were required to press button to respond to the direction of the target arrow within a response window of 1700 ms. They were also required to quickly return eyes to central fixation after making a response when in the overt block. Upper right: Illustration of the 2 (Orienting:

overt, covert) × 2 (Cueing: endogenous, exogenous) task design. The orienting conditions are indicated by the color of the fixation across (green: Overt, red: Covert), which remained during each task block consisted of 8 trials. The cueing conditions were indicated by an arrow superimposed on the fixation cross location (Endogenous), or a change in luminance of one of the circles (Exogenous).

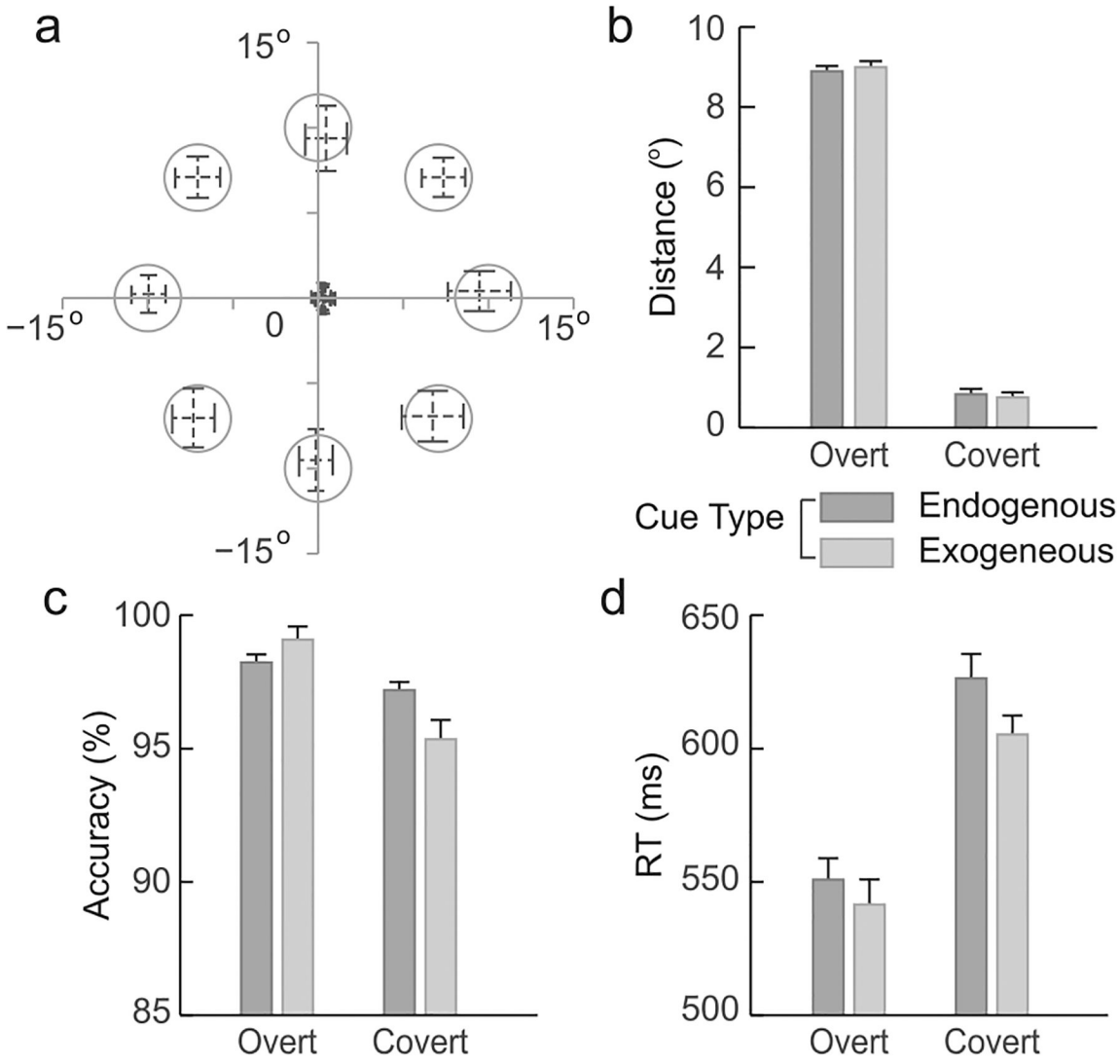

Figure 2.

Eye-movement and behavioral performance in each task condition. The mean and standard deviation (SD) of the coordinates of eye movements (indicated respectively as the center and the boundary of each dashed cross) in trials with the cue appeared at each of the 8 locations in the overt condition and the center focus in the covert condition (a). Distance of eye movements from the center of screen as visual angle (b), response accuracy (c), and reaction time (RT) (d) in each task condition. Error bars indicate the ± 95% confidential interval (CI) for within-subject design across participants.

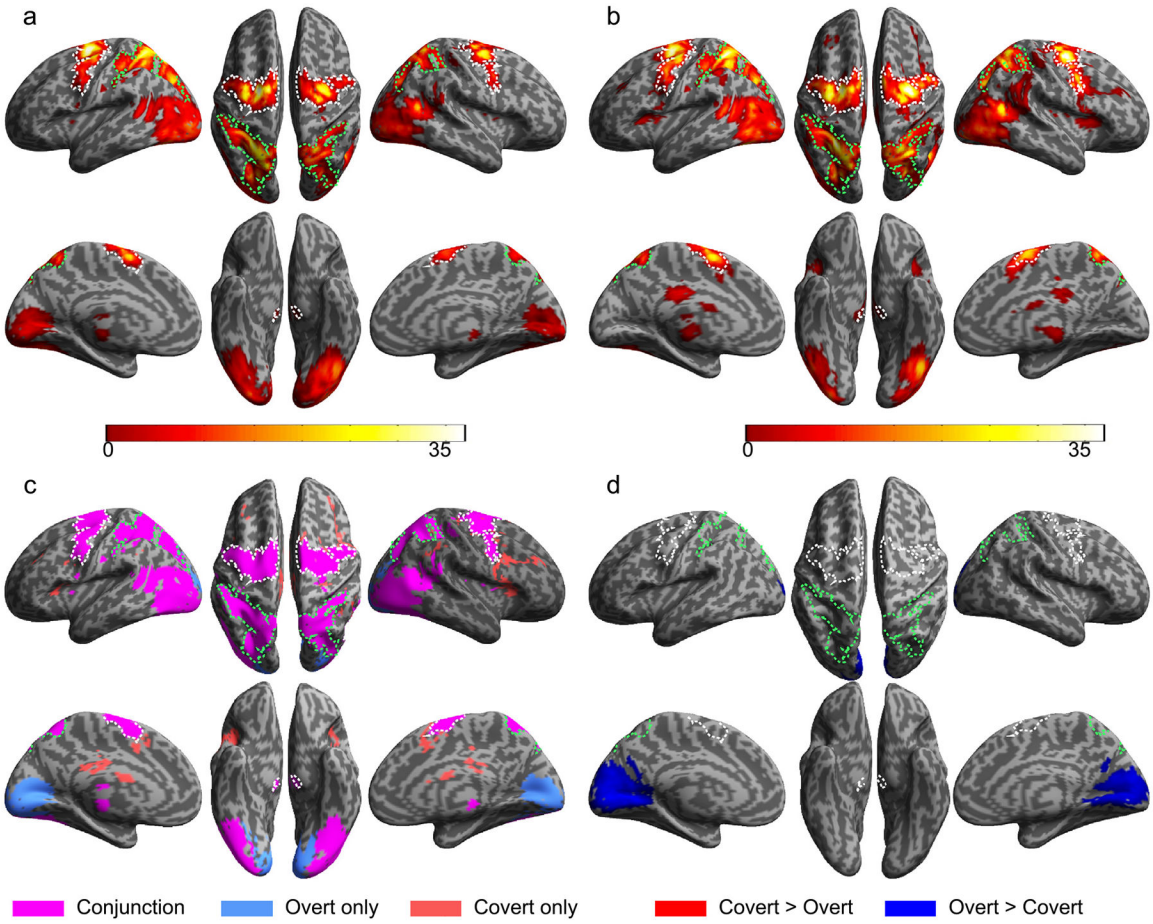

Figure 3.

Brain activation associated with overt and covert orienting of attention. Brain regions that showed significant activation in the contrasts of overt-minus-fixation-baseline (a) and covert-minus-fixation-baseline (b). Colormap indicates the T value. Brain regions that showed significant activation in conjunction and disjunction between these two contrasts (c). Violet: conjunction. Light blue: overt specific activation. Magenta: covert specific activation. Brain regions that showed significant activation changes in the contrast of overt > covert (blue) (d). No region showed significant activation change in the contrast of covert > overt. The frontal and parietal clusters of the frontoparietal network (FPN) identified in the conjunction analysis were highlighted as the areas within the white and green dashed contours, respectively.

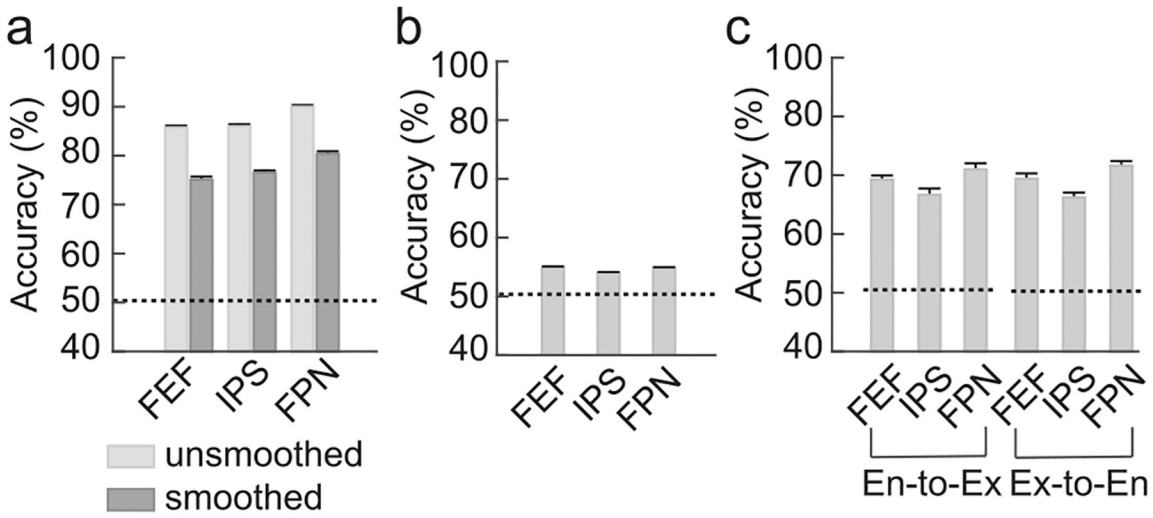

Figure 4.

Accuracy of the overt versus covert classification based on the activation pattern of the voxels in the FPN. (a) Classification accuracy based on the activation of the voxels in the FEF, the IPS, and the FPN (i.e., with FEF and IPS combined). Classification accuracy based on the unsmoothed and smoothed voxels were presented using light and dark grey bars, respectively. (b) Accuracy of the cross-subject classification. (c) Accuracy of the cross-cueing classification for endogenous-to-exogenous (En-to-Ex) and exogenous-to-endogenous (Ex-to-En). The dashed lines represent the chance level accuracy. Error bars indicate the ± 95% confidence interval (CI) for within-subject design across participants.

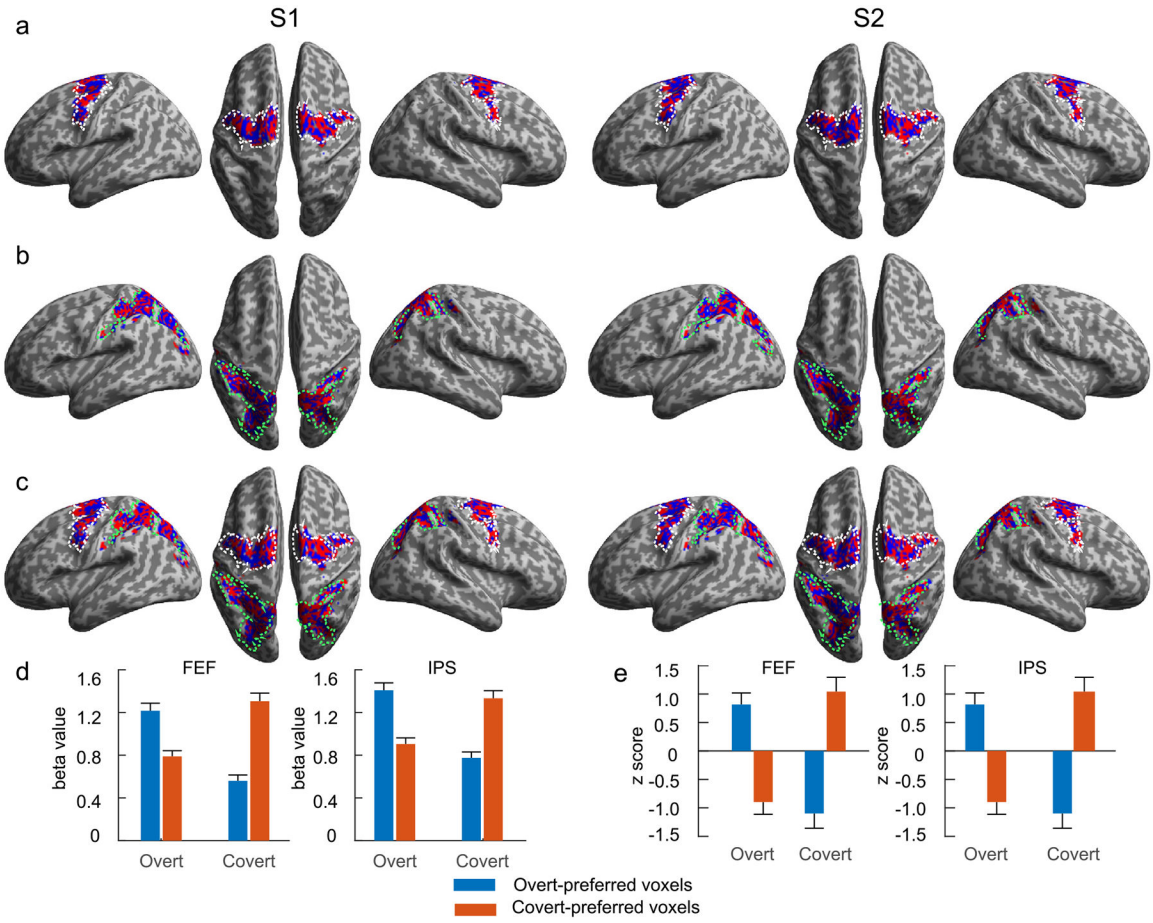

Figure 5.

Weight maps of the overt versus covert classification of two participants. Left and right panels are for the participant S1 and participant S2, respectively. Voxels with SVM weight values significantly below (in blue, overt-preferred) and above (in red, covert-preferred) zero in the classification in the FEF solely (a), in the IPS solely (b), and in the FPN, i.e., FEF and IPS combined (c). The cluster of the FEF and IPS was highlighted as the areas within the white and green dashed contours, respectively. Mean fMRI activation (d) and its z score (e) in voxels with negative weights (overt-preferred) and positive weights (covert-preferred). Error bars indicate the ± 95% CI for within-subject design across participants.

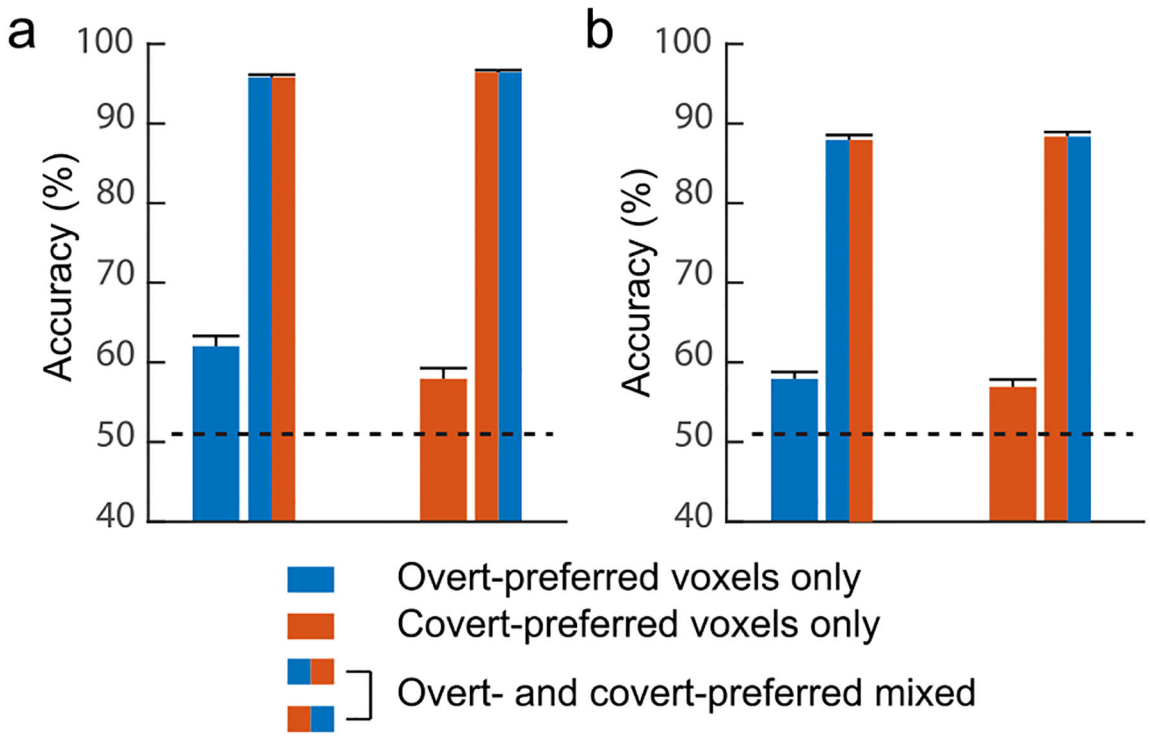

Figure 6.

Classification accuracy based on activation of overt-preferred and covert-preferred voxels. Based on voxels in the FEF (a) and the IPS (b). Blue bar: overt-preferred voxels only. Red bar: covert-preferred only. Blue-red bar: overt- and covert-preferred voxels mixed, with the number of voxels equal to the number of overt-preferred voxels. Red-blue bar: overt- and covert-preferred voxels mixed, with the number of voxels equal to the number of covert-preferred voxels. Dashed line: chance level accuracy. Error bars indicate the ± 95% CI for within-subject design across participants.

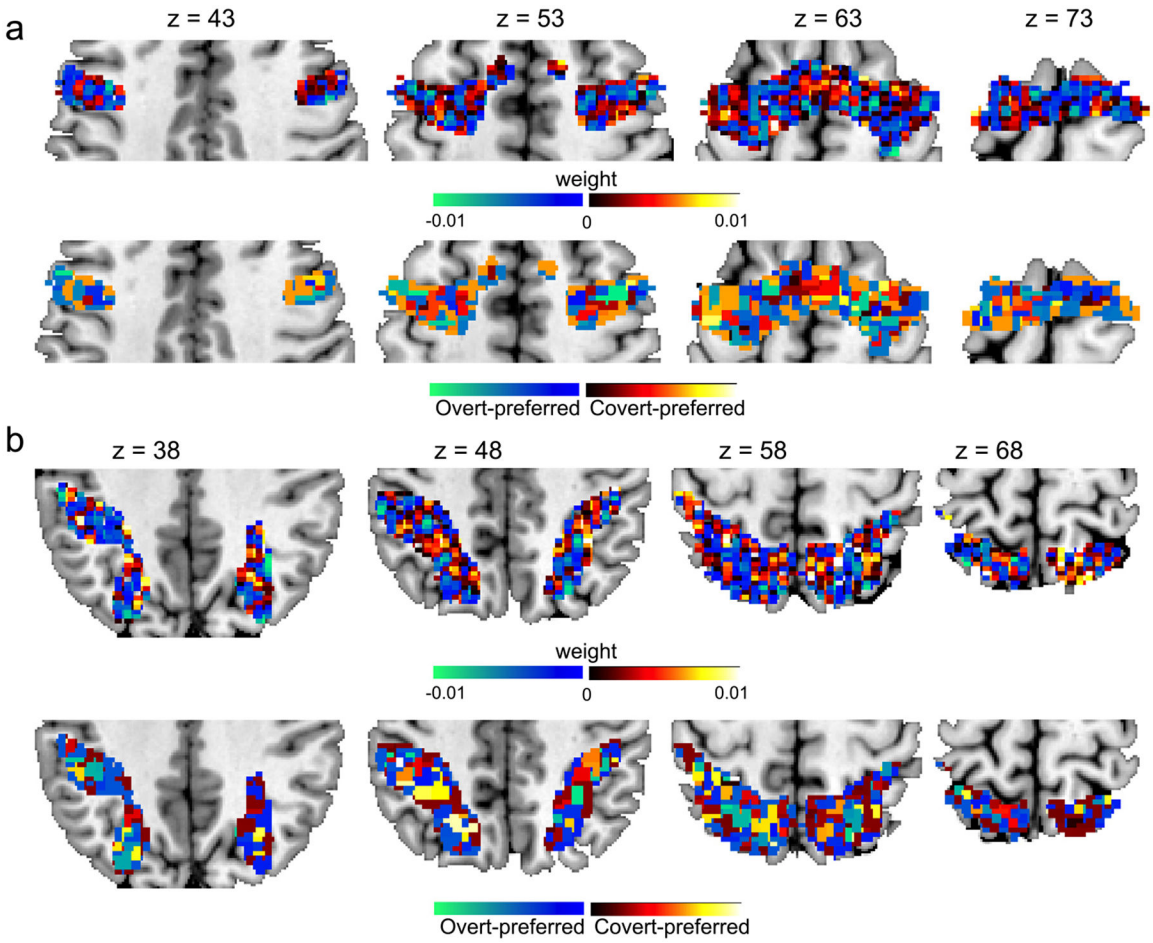

Figure 7.

Topological properties of the weight maps. Axial view of the weight map (upper panel; color map indicates the weight value) and its Morse decomposition (lower panel; color maps indicates the type of cluster) of the FEF (a) and IPS (b) of participant S1.